american physiological society

JNP JOURNAL OF NEUROPHYSIOLOGY

J Neurophysiol 133: 299–309, 2025.
First published December 20, 2024; doi:10.1152/jn.00354.2024

RESEARCH ARTICLE

Control of Movement

Improving localization and measurements of M-waves using high-density surface electromyography

Ernesto H. Bedoy,[1,2,3,7] Efrain A. Guirola Diaz,[5] Ashley N. Dalrymple,[3,7,9,10] Isaiah Levy,[6] Thomas Hyatt,[3,7] Darcy M. Griffin,[2,7,8] George F. Wittenberg,[1,2,4,6] and Douglas J. Weber[2,3,7,8]

[1]*Center for Neuroscience, University of Pittsburgh, Pittsburgh, Pennsylvania, United States;* [2]*Center for Neural Basis of Cognition, University of Pittsburgh and Carnegie Mellon University, Pittsburgh, Pennsylvania, United States;* [3]*Department of Mechanical Engineering, Carnegie Mellon University, Pittsburgh, Pennsylvania, United States;* [4]*Department of Neurology, University of Pittsburgh, Pittsburgh, Pennsylvania, United States;* [5]*Department of Neuroscience, University of Pittsburgh, Pittsburgh, Pennsylvania, United States;* [6]*Department of Physical Medicine and Rehabilitation, University of Pittsburgh School of Medicine, Pittsburgh, Pennsylvania, United States;* [7]*NeuroMechatronics Lab, Carnegie Mellon University, Pittsburgh, Pennsylvania, United States;* [8]*Neuroscience Institute, Carnegie Mellon University, Pittsburgh, Pennsylvania, United States;* [9]*Department of Biomedical Engineering, University of Utah, Salt Lake City, Utah, United States; and* [10]*Department of Physical Medicine and Rehabilitation, University of Utah, Salt Lake City, Utah, United States*

Abstract

Surface electromyography (sEMG) is useful for studying muscle function and controlling prosthetics, but cross talk from nearby muscles often limits its effectiveness. High-density surface EMG (HD-sEMG) improves spatial resolution, allowing for the isolation of M-waves in the densely packed forearm muscles. This study assessed HD-sEMG for localizing M-waves and evaluated the impact of spatial filters on cross talk reduction. We administered peripheral nerve stimulation to activate forearm muscles in five participants. We analyzed cross talk by correlating the shape of M-waves between electrodes and used ultrasound to confirm muscle identity and location. At low-stimulation intensities, we successfully isolated M-waves with minimal cross talk without spatial filtering. Higher recruitment levels produced significant cross talk, which was reduced by applying bipolar or tripolar spatial filters. M-waves from the monopolar HD-sEMG montage showed high correlations between electrodes ($r = 0.97$ transversely; $r = 0.95$ longitudinally), while bipolar and tripolar montages showed lower correlations (bipolar: $r = 0.41$ transversely; $r = 0.19$ longitudinally; tripolar: $r = 0.17$ transversely; $r = 0.01$ longitudinally). The tripolar filter significantly reduced cross talk (51.10% amplitude decay one electrode away) compared with no filter (10.32% amplitude decay one electrode away), effectively reducing cross talk to negligible levels at distances $\geq$2.55 cm. Ultrasound was crucial for distinguishing true activation from artifacts caused by converging signals along muscle boundaries. Spatially filtered HD-sEMG accurately detects and isolates M-waves in the forearm, and ultrasound imaging is useful for verifying the location and identity of the muscles underlying the HD-sEMG grids.

NEW & NOTEWORTHY This study introduces an innovative approach to enhancing evoked potential measurements using high-density surface electromyography (HD-sEMG). The precision and localization of evoked potentials are significantly improved by spatial filters and ultrasound imaging, offering a novel method for better assessing motor pathway integrity. These advancements could lead to more accurate tools for detecting and treating neurological deficits, making it a significant contribution to neurophysiological research.

cross talk; high-density electromyography; M-waves; peripheral nerve stimulation; ultrasound

INTRODUCTION

Stroke and spinal cord injury often damage the neural circuits controlling muscle activity and are the leading causes of paralysis (1–3). Surface electromyography (sEMG) is used to measure muscle activation and changes in recruitment patterns after neurological injury. Understanding these changes may aid in developing motor rehabilitation tools (4, 5).

Motor-evoked potentials (MEPs), generated by stimulating the brain or spinal cord, and compound muscle action

Correspondence: D. J. Weber (dougweber@cmu.edu).
Submitted 12 August 2024 / Revised 11 December 2024 / Accepted 16 December 2024

potentials (CMAPs), including M-waves, produced by peripheral nerve stimulation, are measured by their amplitude, a key indicator of neuromuscular function (6–8). However, cross talk from nearby muscles can distort amplitude measurements (9–12), especially in the forearm where muscles are closely positioned and overlap.

Most MEP and M-wave studies use bipolar sEMG electrodes (9). When measuring evoked responses from a single muscle location, it is impossible to definitively determine whether the sEMG signal originates from the target muscle or a neighboring muscle. Furthermore, the amplitude of target muscle signals themselves can be distorted by cross talk signals (13).

High-density sEMG (HD-sEMG) offers more accurate measures of MEP/M-wave amplitude by providing better coverage of the target muscle and allowing the application of spatial filters to improve the isolation of signal sources. Spatial filters combine signals from multiple electrodes to amplify the desired signal while suppressing interference from nearby muscles (14). The bipolar montage records the voltage difference between two adjacent electrodes while the tripolar montage takes this a step further by measuring the difference between two bipolar signals, enhancing signal isolation. Despite the preference for spatial filtering techniques in HD-sEMG studies, monopolar processing is still used in some applications. For example, studies have used monopolar HD-sEMG to control prosthetic limbs (15) and assess muscle function during gestures (16) and dynamic contraction conditions (17, 18), where capturing the full extent of muscle engagement is prioritized over reducing cross talk.

This paper evaluates a technique for isolating M-waves from multiple muscles using HD-sEMG. We generated M-waves in five able-bodied subjects by applying single pulses of electrical stimulation to peripheral nerves in the arm. We then assessed how well the bipolar and tripolar montages reduced cross talk, with the monopolar montage (without spatial filtering) serving as the control. The tripolar montage provided more effective cross talk reduction. After the stimulation trails, we used ultrasound imaging to accurately identify the muscles beneath the HD-sEMG grids.

These results highlight key challenges in measuring muscle recruitment, particularly in areas where several muscles are close together. Although HD-sEMG provides better coverage of target muscles, careful signal processing is required to detect and eliminate cross talk, ensuring more accurate measurements of muscle activity.

METHODS

Participants

Five right-handed able-bodied volunteers (3 males; ages 24–40, mean = 30.4 yr) provided informed written consent to participate in this study (Table 1). Inclusion criteria included being 18–70 yr old, medically stable, with normal or corrected vision, no neurological or motor impairments, no implanted devices, serious medical conditions, or joint deformities, and the ability to provide informed consent. All participants completed the study. All experimental procedures were approved by the Institutional Review Board at Carnegie Mellon University.

Table 1. *Subject demographics, forearm circumferences, and number of HD-sEMG grids placed around the forearm for musculature mapping*

Subject ID #	Sex	Age, yr	*Forearm Circumference, cm	Number of HD-sEMG Grids
1	Male	40	27.83 ± 1.15	4
2	Female	26	21.87 ± 1.46	3
3	Male	24	28.03 ± 1.33	4
4	Female	38	20.83 ± 1.61	3
5	Male	24	22.60 ± 1.64	3

*Forearm circumferences were calculated by averaging three measurements taken at the proximal end, center, and distal end of the HD-sEMG.

HD-sEMG Electrode Placement and Recording

We recorded muscle activity from each subjects' right forearm at 4,000 Hz using HD-sEMG electrode grids (SAGA 64 +, TMSi, Oldenzaal, Netherlands) comprising 64 Ag | AgCl electrodes (diameter = 4.5 mm; interelectrode distance = 8.75 mm) (Fig. 1*A*). The 8×8 grid spans ~7 cm on each side, covering multiple forearm muscles (19). After cleaning the forearm, ankle, and wrist with abrasive gel (Lemon Prep, Mavidon, Flat Rock, NC) we applied conductive gel (Signa Gel, Parker, NJ) to each electrode. The HD-sEMG grids were then positioned around the forearm, with ground electrodes on the ankle and reference electrodes on the wrists.

Cross Talk Study

We placed one HD-sEMG grid on the anterior forearm, 1 cm medial to the biceps tendon, and an average of 3.88 cm (range: 3.5–4.5 cm) distal to the elbow crease. We electrically stimulated the median nerve to selectively recruit muscles in this area using the monophasic, cathodal pulses (1 ms pulse width) at a 1-Hz repetition rate with a DS8R constant current stimulator (Digitimer Ltd, Welwyn Garden City, Hertfordshire, UK). A custom MATLAB (MathWorks, Natwick, MA) script controlled the stimulator output, which generated a 5 V trigger at each stimulation pulse, recorded as a digital event input on the HD-sEMG system. We identified the twitch threshold as the lowest intensity at which muscle twitches were first observed. We generated recruitment curves by measuring M-waves across a range of stimulation amplitudes, starting 1 mA below the twitch threshold up to each participant's maximum comfort level. We repeated each intensity level 10 times in a random order, with all intensities delivered once before starting the next repetition.

Forearm Musculature Mapping Test

After the cross talk study, we mapped M-waves in multiple forearm muscles by placing 3–4 HD-sEMG grids around the forearm. The ulnar, anterior, and posterior grids were positioned over the ulnar muscles [extensor carpi ulnaris (ECU) and flexor carpi ulnaris (FCU)], the anterior forearm, and the posterior forearm, respectively. We used an additional grid for subjects with larger forearm circumferences, while the anterior grid retained its position from the *Crosstalk Study*. The other grids were aligned adjacent to the anterior grid (Fig. 1*B*). We electrically stimulated the median, ulnar, and radial nerve individually to selectively recruit target muscles (20).

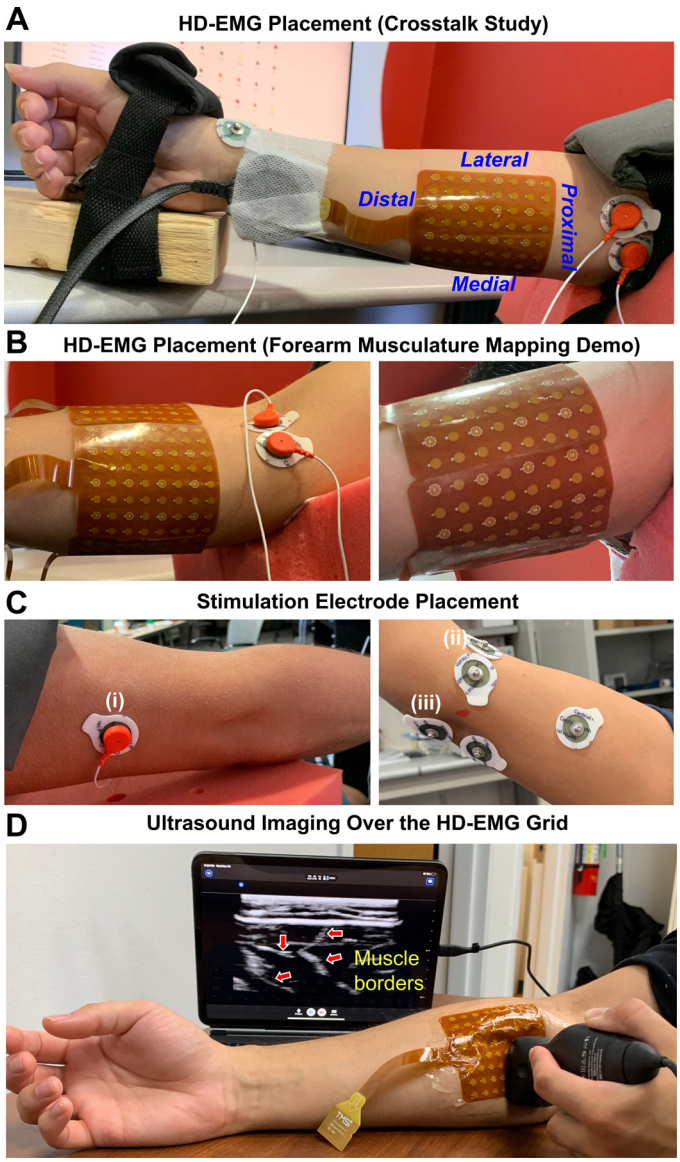

Figure 1. Experimental setup and ultrasound-guided muscle boundary identification. *A*: we placed an HD-sEMG grid on the anterior forearm while participants held a neutral pose. A block supported the wrist and elbow to avoid pressure on the grid, and we secured the upper arm and hand with straps. *B*: we positioned 3–4 HD-sEMG grids around the forearm. *C*: we stimulated the radial nerve near the lateral humerus (*i*), the medial nerve at the elbow crease (*ii*), and the ulnar nerve between the medial epicondyle and olecranon (*iii*) using bipolar electrodes. *D*: we identified muscle boundaries beneath the HD-sEMG grids with ultrasound imaging (red arrows). HD-sEMG, high-density surface electromyography.

Stimulation Electrode Placement

Median nerve stimulation.

We placed electrodes along the elbow crease (21), positioning the cathode 2 cm medial to the biceps tendon (2.5 cm for one participant) and the anode 2.5 cm medial to the cathode (Fig. 1*C*). We stimulated in steps of 3 mA from 3 mA to 24 mA ($n = 2$) or 30 mA ($n = 2$). For *subject 2*, the range was 2–12 mA in steps of 2 mA. This stimulation targeted the flexor carpi radialis (FCR), pronator teres (PT), palmaris longus (PL), and flexor digitorum superficialis (FDS).

Ulnar nerve stimulation.

We placed electrodes near the elbow with the cathode between the medial epicondyle and olecranon, and the anode was positioned proximal-medial to the cathode (Fig. 1*C*). Stimulation ranged from 3 mA to 18 mA ($n = 3$) or 24 mA ($n = 1$) in steps of 3 mA. For *subject 2*, the range was 2–10 mA in steps of 2 mA. This stimulation targeted the FCU and flexor digitorum profundus (FDP).

Radial nerve stimulation.

We placed electrodes on the upper arm with the cathode positioned 7 cm proximal to the lateral epicondyle (the offset was 0.5 cm lateral for *subject 1*) and the anode on the inner arm opposite to the cathode (Fig. 1*C*). Stimulation intensity ranged from 3 mA to 18 mA ($n = 1$), 24 mA ($n = 1$), or 30 mA ($n = 3$), in steps of 3 mA. This stimulation targeted the brachioradialis (Brach), extensor carpi radialis (ECR), extensor digitorum communis (EDC), and ECU.

HD-sEMG Processing and Analysis

We processed HD-sEMG data using custom MATLAB code. We removed the stimulation artifact by excluding data from 2 ms before to 5 ms after the pulse onset and filling the gap with linear interpolation. Then, we applied a second-order 10-Hz high-pass Butterworth filter. We quantified M-wave amplitude as the peak-to-peak value within a time window that excluded late responses like H-reflexes and F-waves. We measured M-waves between 5 and 30 ms after stimulation in the monopolar montage for all subjects and in the spatially filtered montages for *subject 1* due to longer-latency M-waves. For the remaining spatially filtered montages, the measurement window for the M-waves was 5–16 ms.

We used the average peak-to-peak amplitudes for each electrode across trials to build recruitment curves. We defined the activation threshold (AT) as the intensity at which amplitude exceeded 5% of the maximum amplitude, and the maximal motor response (Mmax) as the intensity where the recruitment curve saturated, with less than 2% amplitude change. As different muscle regions had varying recruitment profiles, we reported the median AT and Mmax. We excluded electrodes with excessive noise, artifacts, or no signal, pruning 5% of electrodes (0–11% per grid).

Topographic heat maps.

We generated topographic heat maps of M-wave peak-to-peak amplitudes from all HD-sEMG electrodes at each stimulation intensity (Fig. 2). Contour heat maps displayed the normalized amplitudes, with hotspots identified as areas of larger peak-to-peak values. For excluded electrodes, we substituted the mean value of adjacent electrodes in the medial-lateral direction. If the excluded electrode was on the grid edge, we used the value of the nearest electrode. These adjustments were made solely for visualization.

Cross talk detection.

We calculated linear correlation coefficients between electrode pairs along rows (transverse) and columns (longitudinal) to detect cross talk. A correlation above 0.9 indicated cross talk. Across all subjects, trials, and stimulation levels,

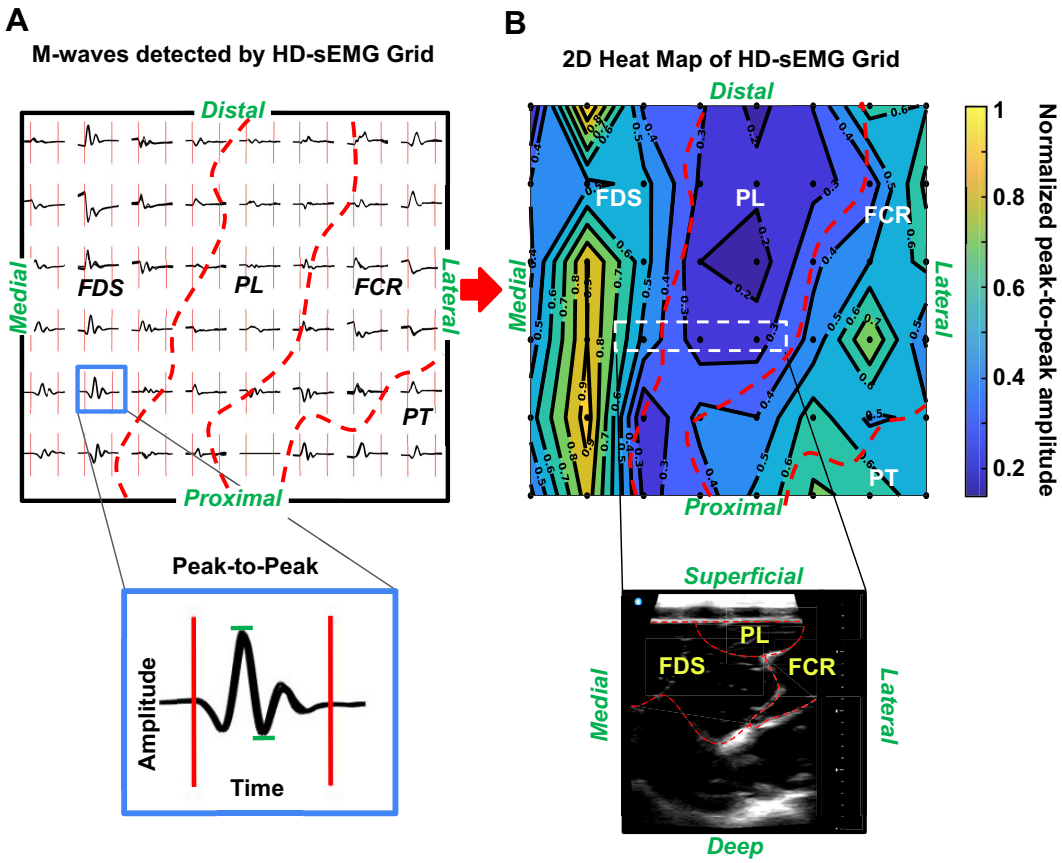

Figure 2. Topographic heat map generation and ultrasound-guided muscle identification. Example data from *subject 1* with the tripolar montage. *A*: we plotted M-waves relative to the HD-sEMG placement on the forearm (stimulation amplitude = 24 mA). We obtained peak-to-peak amplitude (distance between horizontal green bars) within the time window of interest (vertical red bars). *B*: we generated 2-D topographic heat maps with a color scale representing amplitudes (blue = low; yellow = high). Using ultrasound guidance, we mapped muscle boundaries (red dashed lines). The white dotted rectangle, representing the ultrasound field of view, spans approximately three electrodes. HD-sEMG, high-density surface electromyography.

there were 65,163 (monopolar), 52,010 (bipolar), and 42,994 (tripolar) observations in the transverse direction, and 65,163 (monopolar), 44,740 (bipolar), and 31,026 (tripolar) in the longitudinal direction. We plotted the cumulative distribution function (CDF) of the correlation coefficients for each direction.

M-wave source localization.

After stimulation, we applied ultrasound gel (Pro Advantage, Portland, TN) and used a portable ultrasound probe (Butterfly IQ, Matamoros, Mexico) to locate muscles beneath the HD-sEMG electrodes (Figs. 1*C* and Fig. 2*B*). The source electrodes were those within the ultrasound-defined muscle boundary and with M-wave amplitudes at least 50% of the maximum recorded for that muscle. To minimize the effect of cross talk, we limited monopolar montage localization to the highest stimulation level where correlations stayed below 0.9. For bipolar and tripolar montages, we localized at Mmax or the highest stimulation level if Mmax was not reached.

Amplitude decay.

Cross talk amplitude decays rapidly with distance from the source electrode (9, 22, 23). We calculated decay as the percent reduction in signal amplitude at one electrode distance from the source. We also measured cross talk at increasing distances from the source. These values were averaged across all stimulation intensities at or above the AT, with a focus on the muscle with the lowest AT to minimize interference from adjacent muscles (Fig. 3). Only intensities up to Mmax for the muscle with the lowest AT were used in the calculation to further mitigate cross talk from adjacent muscles. Electrode selection was guided by the tripolar montage due to its effectiveness in isolating muscle activity. The threshold for negligible cross talk was defined as a 15% reduction in M-wave amplitude from the source electrode (7). Due to excessive muscle activation, amplitude decay could only be assessed in two subjects (*subjects 1* and *5*).

RESULTS

Visualizing Cross Talk in Muscle Activity Maps

We stimulated the median nerve to evoke responses in the anterior forearm muscles. Figure 4 shows heat maps that highlight the impact of cross talk and how spatial filtering reduces it. With the monopolar montage, activation maps for the FDS and FCR muscles began to merge at higher stimulation intensities, making it difficult to separate their contributions. However, applying spatial filtering kept the activation

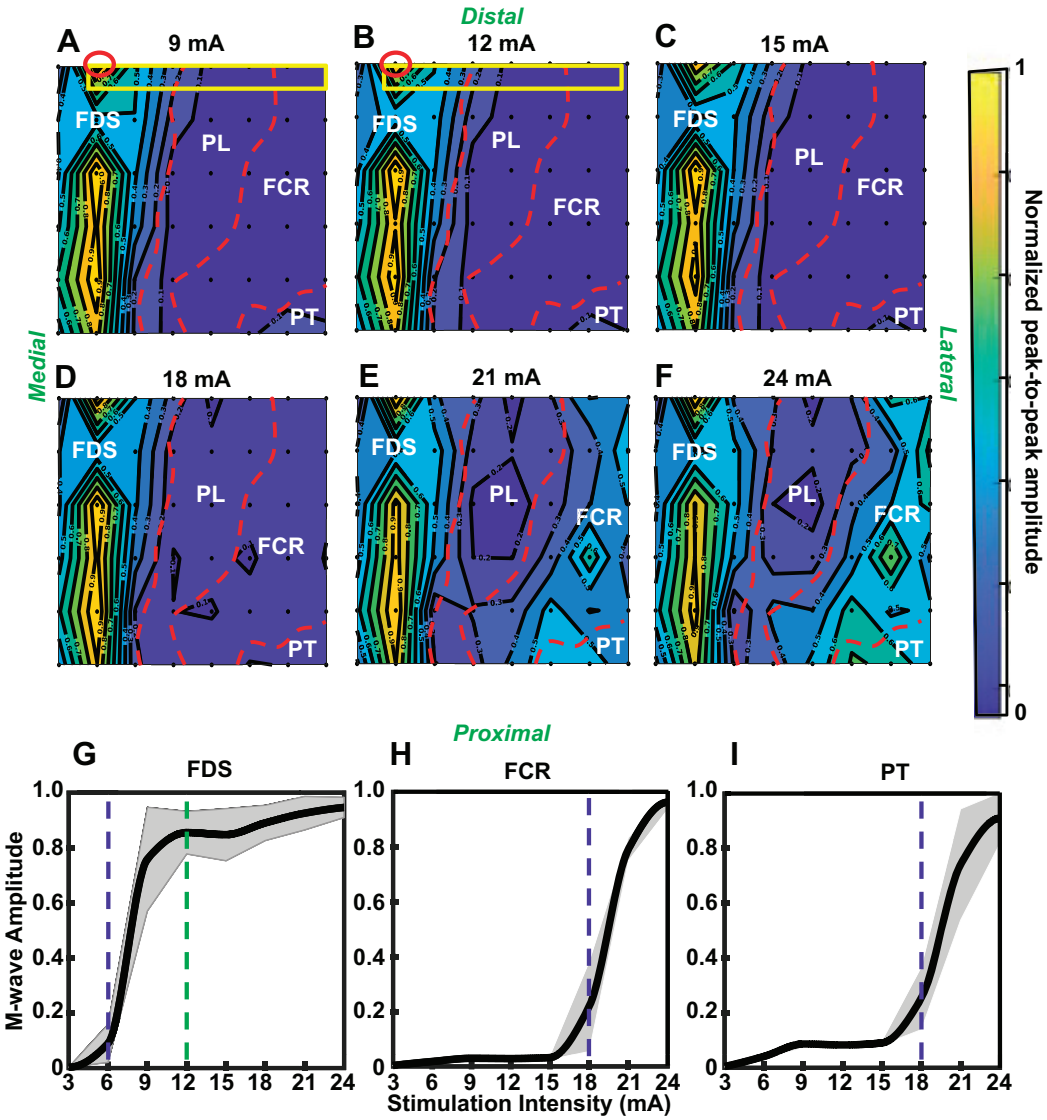

Figure 3. Topographic heat maps of M-wave amplitudes (tripolar montage) at increasing stimulation intensities and recruitment curves of *subject 1*. The HD-sEMG grid covered the FDS, PL, FCR and PT muscles. *A* to *F* display M-wave amplitudes at increasing stimulation levels, while *G* to *I* present recruitment curves for the FDS, FCR, and PT muscles. FDS reached Mmax at 12 mA (green dashed line), while FCR and PT reached the greatest change at 18 mA (blue dashed line) without reaching Mmax. The yellow rectangle on the distal end of the grid (*A* and *B*) marks the electrodes used to calculate amplitude decay from the source electrode, indicated by the red circle. We normalized the peak-to-peak amplitude to the maximum for each intensity to highlight PT muscle activity at lower stimulation levels. Ultrasound examination over the HD-sEMG identified muscle boundaries (red dashed lined). FCR, flexor carpi radialis; FDS, flexor digitorum superficialis; HD-sEMG, high-density surface electromyography; PL, palmaris longus; PT, pronator teres.

zones distinct, reducing cross talk and improving muscle differentiation.

Measuring and Eliminating Cross Talk

We quantified cross talk by calculating the correlation between M-waves measured on pairs of electrodes in the transverse and longitudinal directions. We aggregated the results across trials, intensities, and participants. In the transverse direction, over 81.9% of correlations in the monopolar montage were greater than 0.9 (Fig. 5), indicating high cross talk. In contrast, 82.6% and 93.7% of correlations in the bipolar and tripolar montages, respectively, were less than 0.9, showing that spatial filtering effectively reduces cross talk.

In the longitudinal direction, correlation values in the bipolar and tripolar montages were weaker due to action potential propagation (88.5% and 98% of correlations were less than 0.9, respectively). However, time-aligning action potentials increased correlation values beyond 0.9, similar to the monopolar montage (Supplemental Fig. S6). This shows that propagation effects are masked by cross talk in the monopolar montage.

We also measured cross talk through amplitude decay. In the monopolar montage, amplitude decayed minimally (10.32 ± 5.30%), while decay was greater in the bipolar (35.43 ± 10.49%) and tripolar (51.10 ± 8.10%) montages, confirming the spatial filters' effectiveness in reducing cross talk. Finally, we defined cross talk's spatial extent as

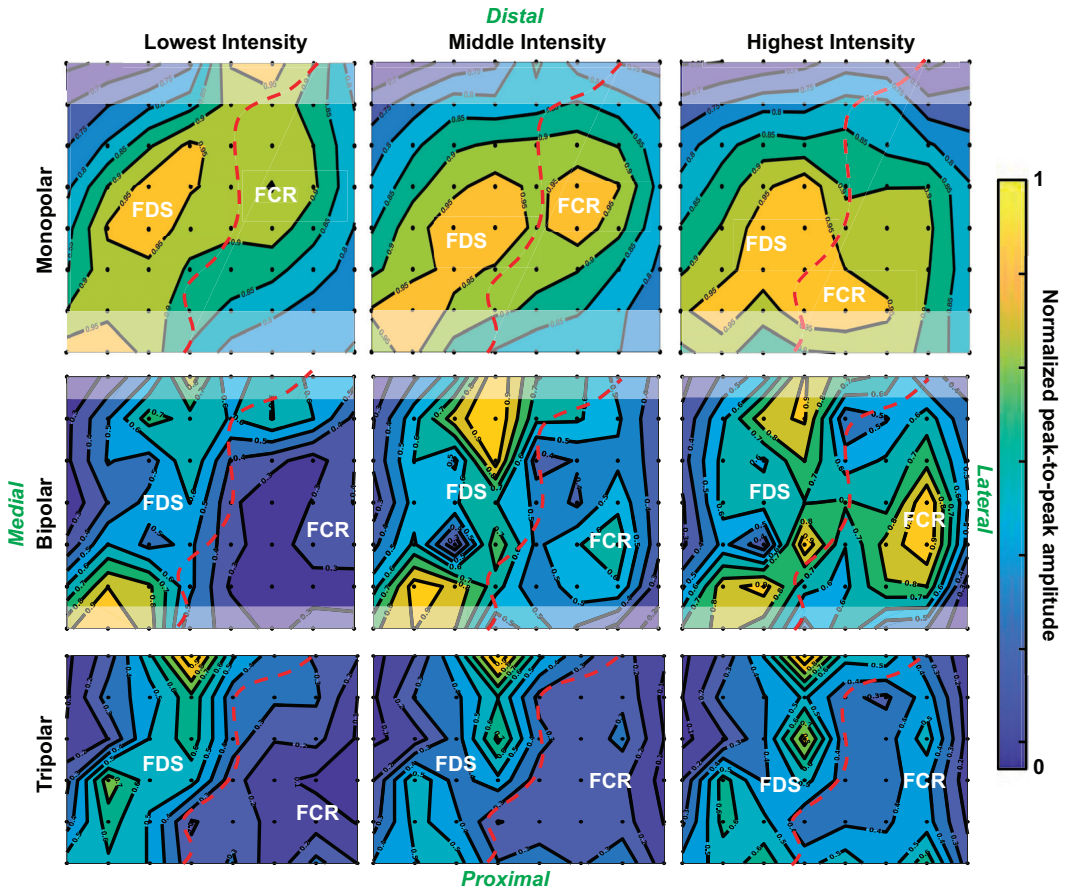

Figure 4. Cross talk effects on sEMG amplitude and muscle activation patterns as stimulation intensity increases. Heat maps show M-wave amplitude at each electrode normalized to the maximum amplitude for each condition (*subject 2*). Grayed-out portions of the monopolar and bipolar heat maps account for the loss of electrodes from the differentiation in the bipolar and tripolar montages. We used ultrasound imaging to identify muscle boundaries (indicated by red dashed lines) within the regions covered by the HD-sEMG grids. HD-sEMG, high-density surface electromyography.

the distance from the M-wave source to the nearest electrode with negligible cross talk. The spatial filters were the only methods that achieved negligible cross talk, with the bipolar montage reaching this level between 3 and 5 electrodes (2.55–4.25 cm) and the tripolar montage between 2 and 3 electrodes (1.70–2.55 cm) (Fig. 6).

Removing Cross Talk's Effect on Recruitment Curves with Spatial Filters

Cross talk also affected recruitment curves. Although the bipolar and tripolar montages produced similar recruitment curve shapes, the monopolar montage displayed altered

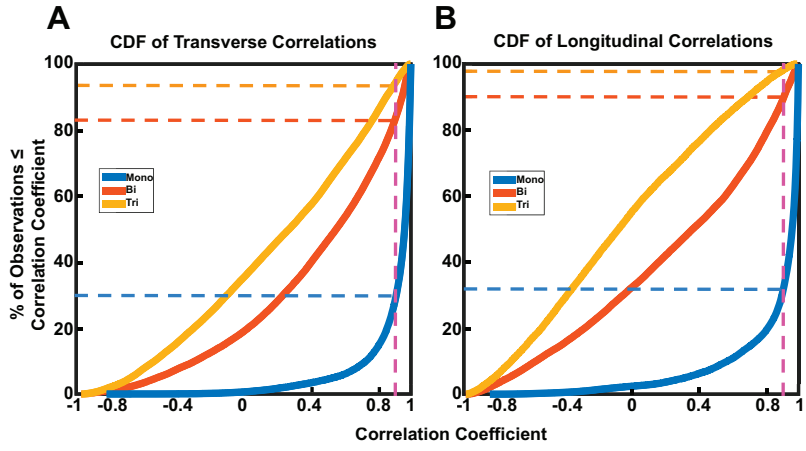

Figure 5. M-wave correlation coefficients across electrodes with different spatial filters. We aggregated cumulative distribution functions (CDFs) of M-wave correlation coefficients across all subjects. We obtained CDFs for electrodes in the transverse direction (*A*) and longitudinal direction (*B*) for the monopolar (blue), bipolar (red), and tripolar (orange) montages. Dashed lines show where each montage reaches a correlation of 0.9 (magenta).

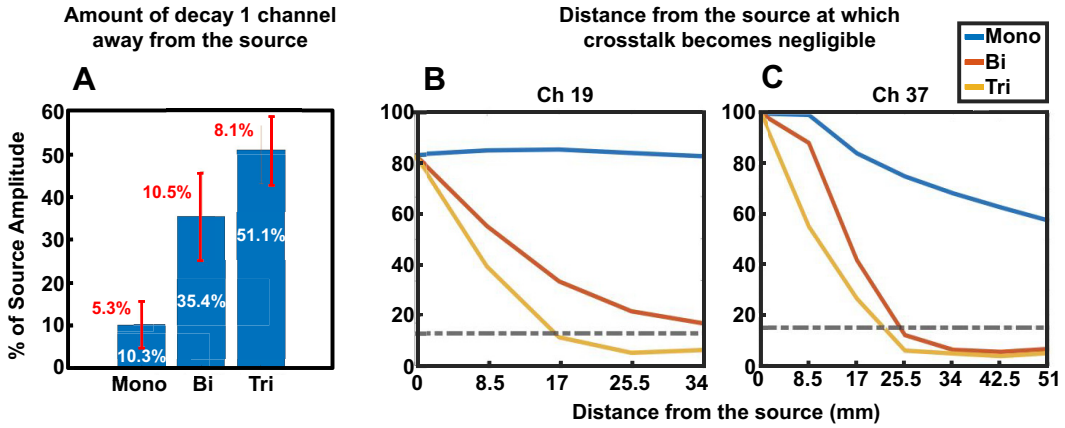

Figure 6. M-wave amplitude decay. *A*: mean and standard deviation of the percent amplitude decay one electrode away from the source for each montage. For each subject, we divided the mean of all electrodes surrounding the source by the mean of all source electrodes. Plots from *B* and *C* for *subject 5* and *subject 1*, respectively, show where the peak-to-peak M-wave amplitude drops below 15% of the source amplitude (gray dotted line).

curves (Fig. 7) due to a lower AT. Spatial filtering corrected these distortions, demonstrating the filters' effectiveness in producing reliable recruitment curves. These distortions and corrections are evident in Table 2, where the AT values align closely for the bipolar and tripolar montages but deviate notably for the monopolar montage.

Applying Ultrasound Imaging to Visualize the Muscle Under Each Hotspot

The diverse muscle recruitment patterns seen in the tripolar montage heat maps were colocalized with ultrasound to define muscle boundaries (Fig. 8). Although heat maps alone could separate two muscles, identifying distinct sources became harder as more muscles were recruited (Fig. 8*C*). Cross talk remained an issue between 2 and 3 electrodes (1.7–2.55 cm) from the source (Fig. 6), especially near muscle boundaries, where overlapping responses from surrounding muscles created artificial peaks (Fig. 9). Ultrasound imaging was essential for distinguishing muscle responses from bellies versus boundaries.

Mapping Muscle Activation Across the Full Circumference of the Forearm

We generated activation maps using HD-sEMG grids around the entire forearm, capturing specific muscle group activations in response to nerve stimulation (Supplemental Fig. S1–S5). Median nerve stimulation activated the FDS and FCR muscles, ulnar nerve stimulation activated the FCU and lateral FDP, and radial nerve stimulation activated the Brach, ECR, and EDC muscles. Ultrasound confirmed the muscle identities and locations beneath the hotspots, validating the maps' accuracy. Contour lines across grids connected smoothly, enabling a full forearm muscle activation map. The tripolar montage significantly improved muscle localization and reduced cross talk compared with the monopolar montage, which showed signal spread across nontarget muscles.

DISCUSSION

We used HD-sEMG combined with spatial filtering techniques to isolate M-wave responses from individual muscles, which were identified through ultrasound imaging. The findings showed that a tripolar montage significantly outperformed monopolar and bipolar configurations in minimizing cross talk. In addition, this approach allowed for precise mapping of forearm musculature by cross-referencing EMG hotspots with muscles identified through ultrasound. This combination of electrical activity localization and anatomical identification provides a more detailed understanding of muscle recruitment, offering valuable insights for neuromuscular studies.

Distinguishing Cross Talk from Muscle Activation

Amplitude measures are critical for studying motor control and identifying neurological markers (6–8). However, cross talk can distort these measures, leading to inaccurate assessments of muscle activation, recruitment properties, and prosthetic control (9, 11, 24). Without cross talk reduction, the resulting sEMG signals may not accurately reflect the true amplitude of muscle activity.

Our findings demonstrated that M-waves measured via the monopolar HD-sEMG montage exhibited high levels of cross talk, as evidenced by high correlation (>90%) and zero-lag propagation in both transverse and longitudinal directions. In contrast, applying bipolar and tripolar spatial filters revealed delayed muscle action potential propagation, significantly reducing correlations (bipolar <20%, tripolar <1%). When accounting for propagation delays, the correlations in the bipolar and tripolar montages increased to match those of the monopolar montage, confirming that the monopolar setup was highly susceptible to cross talk (Supplemental Fig. S6).

Although some researchers question the use of cross-correlation for detecting cross talk due to nonpropagating components (22), our data suggest this concern is minimal at close electrode spacing (8.75 mm). High correlations (≥0.9) were observed in monopolar recordings despite the presence of nonpropagating components, indicating that they do not significantly distort correlation measures at close distances.

After reducing cross talk with spatial filters, amplitude-based measures reliably distinguished between true muscle sources and cross talk. The tripolar montage showed a 51.1% amplitude decay outside source boundaries, characteristic of volume conduction, whereas the monopolar setup exhibited

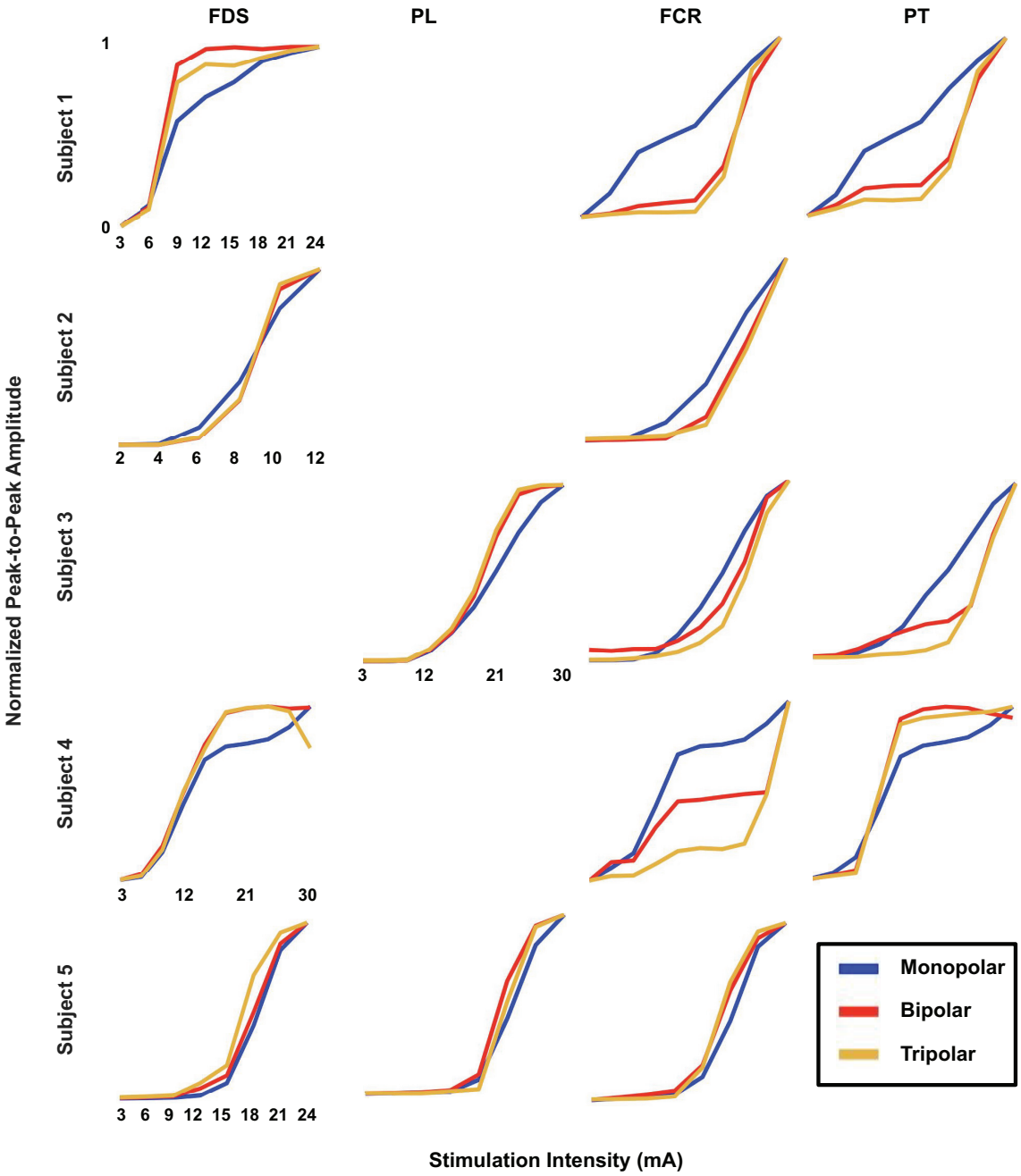

Figure 7. M-wave recruitment curves across montages. We compared recruitment curves for the maximum amplitude electrode at the highest stimulation intensity across montages for each subject. Most subjects showed greater deviation between the monopolar montage (blue) and the tripolar (orange) montages compared with the bipolar (red) and the tripolar montages.

much lower decay, with high correlations suggesting that the sustained amplitude was due to cross talk.

As modern EMG systems can implement these and other types of spatial filters digitally and with minimal computational delay, these methods can be applied in real-time across various applications, including intraoperative neuromonitoring (25). Real-time cross talk reduction enhances the specificity and accuracy of HD-sEMG for monitoring muscle activation, making it highly suitable for dynamic clinical environments.

Improved Accuracy of Cross Talk Measurement

Accurately measuring cross talk during voluntary contractions is challenging due to the difficulty in isolating individual muscles. Our study overcame this limitation by using a more controlled method, employing peripheral nerve stimulation to measure cross talk with greater precision. We observed that cross talk decayed rapidly in the transverse direction using the tripolar montage, falling below 15% of the source amplitude (7) within 1.70–2.55 cm.

Table 2. *M-wave activation thresholds for each montage*

	Subj. 1		Subj. 2		Subj. 3	Subj. 4		Subj. 5	
Median	FDS, mA	FCR, mA	FDS, mA	FCR, mA	FCR, mA	FDS, mA	FCR, mA	FDS, mA	FCR, mA
Mono	3	3	4	4	12	6	6	12	12
Bi	3	15	6	6	18	6	6	12	12
Tri	3	15	6	6	18	6	6	9	12

FCR, flexor carpi radialis; FDS, flexor digitorum superficialis.

Previous studies, such as one examining forearm EMG during gripping, reported slower decay with cross talk only becoming negligible between 3 and 6 cm (26). This discrepancy is likely due to interference from adjacent muscles, which artificially elevated the amplitude in those studies, as illustrated in Fig. 9. In contrast, our findings are consistent with studies on larger muscles, such as the quadriceps, where muscle separation is greater, and cross talk decay is more rapid (27). This highlights the increased accuracy of our method, particularly in regions with closely spaced muscles like the forearm.

Improved Precision in Muscle Mapping

The combination of HD-sEMG and ultrasound imaging enabled precise mapping of muscle activity by combining electrical and anatomical data. This approach allowed us to identify EMG hotspots and map them to specific muscles visualized via ultrasound, providing a detailed spatial representation of muscle recruitment. Unlike single-point measurements in bipolar montages, which are prone to cross talk and offer limited spatial detail, the combination of HD-sEMG and ultrasound gave us a clearer, more complete view of muscle activation. This method significantly enhances the accuracy of muscle mapping, providing valuable insights for neuromuscular studies, motor control research, and clinical applications such as prosthetics, where precise muscle localization is critical.

Limitations

Although the tripolar montage reduces cross talk, it also removes some information from the target muscle (28). As the tripolar montage was applied to all HD-sEMG electrodes, all electrodes were affected equally, thus, amplitude comparisons between muscles remained valid. We did not account for cross talk from deeper muscles, which may require other filtering methods.

Conclusions

Research on the small, interconnected forearm muscles is crucial for advancing our understanding of hand function in both healthy individuals and those with neurological impairments. However, cross talk from adjacent muscles can distort measurements of muscle amplitude and localization,

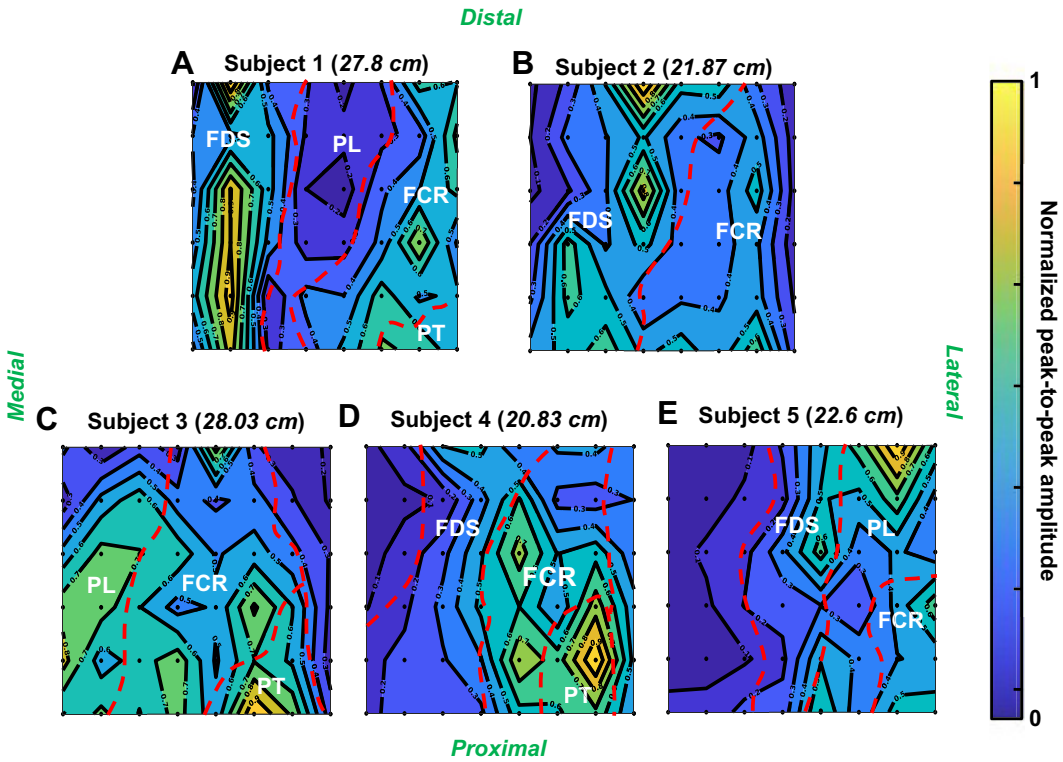

Figure 8. Tripolar topographic heat maps of each subject at Mmax. We normalized the peak-to-peak amplitudes. Ultrasound examination over the HD-sEMG identified muscle boundaries (red dashed lined). FCR, flexor carpi radialis; FDS, flexor digitorum superficialis; HD-sEMG, high-density surface electromyography; PL, palmaris longus; PT, pronator teres.

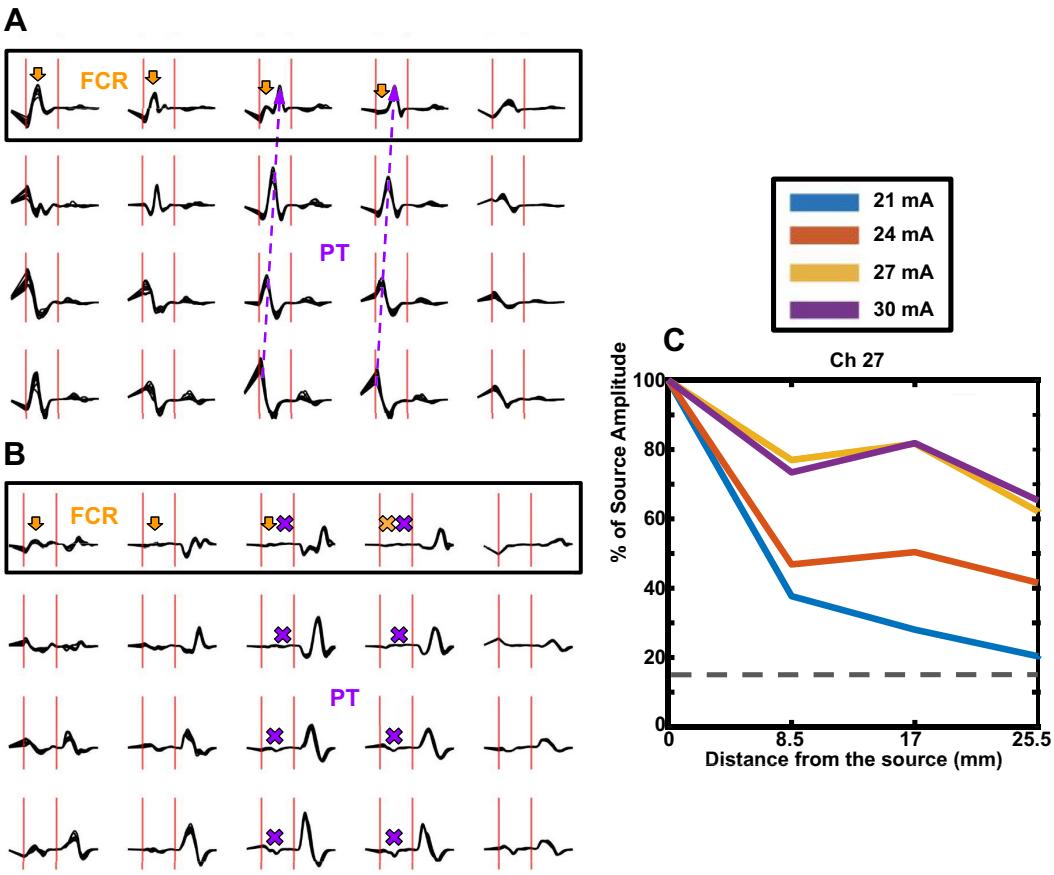

Figure 9. Signal mixing at the muscle boundary. *A*: the tripolar montage time series at 30 mA (0–30 ms, between the two vertical red lines) shows the FCR muscle activating first, with rapid decay away from the source (orange arrow). The PT muscle activates second, shown by the longitudinal signal propagation (purple arrow). Signal mixing from the overlapping FCR and PT signals occurs at the muscle boundary. *B*: at 21 mA, only the FCR muscle activates, shown by the single peak that decays transversely (orange arrow). The PT muscle remains below its activation threshold (purple "X"). *C*: the peak-to-peak amplitude plot tracks the decay of the FCR signal, showing a steep decline at 21 mA. At higher intensities (24–30 mA), PT muscle activation alters the expected decline, as seen in the amplitude rise where the two signals overlap. FCR, flexor carpi radialis; FDS, flexor digitorum superficialis; HD-sEMG, high-density surface electromyography; PL, palmaris longus; PT, pronator teres.

reducing control accuracy in EMG-based prosthetics and affecting the reliability of research results. Our findings demonstrate that the tripolar montage significantly minimizes cross talk, enhancing the precision of muscle activity localization. In addition, combining HD-sEMG with ultrasound imaging enables accurate identification and mapping of forearm muscles. These results highlight the importance of optimizing electrode placement and employing spatial filtering techniques to improve the accuracy of EMG applications, ultimately leading to more consistent and reliable outcomes in both research and clinical settings.

ETHICAL APPROVALS

This study was performed in accordance with the Declaration of Helsinki and approved by the Carnegie Mellon University Institutional Review Board (STUDY2020_00000471). A detailed explanation of the experiment was given to all participants before they gave their informed consent.

DATA AVAILABILITY

Code to plot time series, heat maps and recruitment curves and to reproduce M-wave correlations can be found on: https://github.com/ehbedoy/Process_Mwaves.git. Source data for this study are openly available at: https://doi.org/10.17504/protocols.io.261ger4xyl47/v1.

SUPPLEMENTAL MATERIAL

Supplemental Figs. S1–S6: https://doi.org/10.6084/m9.figshare.27969828.

ACKNOWLEDGMENTS

We thank the participants for volunteering their time to participate in this study. We also thank The BRAIN Initiative of the National Institutes of Health for funding this project.

GRANTS

The research was funded by the NIH The Brain Initiative Diversity Supplement UH3NS100541.

DISCLOSURES

D. J. Weber has ownership interest (stock, stock options, royalty, receipt of intellectual property rights/patent holder, excluding

diversified mutual funds), equity shares, and consulting fees (advisory board) from Bionic Power Inc, Neuroone Inc, Reach Neuro Inc, Neuronoff Inc, and Panther Life Sciences, LLC. None of the other authors has any conflicts of interest, financial or otherwise, to disclose.

AUTHOR CONTRIBUTIONS

E.H.B. and D.J.W. conceived and designed research; E.H.B., E.A.G.D. and T.H. performed experiments; E.H.B. analyzed data; E.H.B., A.N.D., I.L., and D.J.W. interpreted results of experiments; E.H.B. and E.A.G.D. prepared figures; E.H.B. drafted manuscript; E.H.B., E.A.G.D., A.N.D., I.L., D.M.G., G.F.W., and D.J.W. edited and revised manuscript; E.H.B., E.A.G.D., A.N.D., I.L., T.H., D.M.G., G.F.W., and D.J.W. approved final version of manuscript.

REFERENCES

1. **Gordon T**, **Tyreman N.** Sprouting capacity of lumbar motoneurons in normal and hemisected spinal cords of the rat. *J Physiol* 588: 2745–2768, 2010. doi:10.1113/jphysiol.2010.190389.
2. **Milner-Brown HS**, **Stein RB**, **Lee RG.** Pattern of recruiting human motor units in neuropathies and motor neurone disease. *J Neurol Neurosurg Psychiatry* 37: 665–669, 1974. doi:10.1136/jnnp.37.6.665.
3. **Thomas CK**, **Bakels R**, **Klein CS**, **Zijdewind I.** Human spinal cord injury: motor unit properties and behaviour. *Acta Physiol (Oxf)* 210: 5–19, 2014. doi:10.1111/apha.12153.
4. **Peckham PH**, **Knutson JS.** Functional electrical stimulation for neuromuscular applications. *Annu Rev Biomed Eng* 7: 327–360, 2005. doi:10.1146/annurev.bioeng.6.040803.140103.
5. **Rastgoo M**, **Naghdi S**, **Nakhostin Ansari N**, **Olyaei G**, **Jalaei S**, **Forogh B**, **Najari H.** Effects of repetitive transcranial magnetic stimulation on lower extremity spasticity and motor function in stroke patients. *Disabil Rehabil* 38: 1918–1926, 2016. doi:10.3109/09638288.2015.1107780.
6. **Karatzetzou S**, **Tsiptsios D**, **Terzoudi A**, **Aggeloussis N**, **Vadikolias K.** Transcranial magnetic stimulation implementation on stroke prognosis. *Neurol Sci* 43: 873–888, 2022. doi:10.1007/s10072-021-05791-1.
7. **Konrad P.** *The ABC of EMG: A Practical Introduction to Kinesiological Electromyography*. Scottsdale, AZ: Noraxon INC., 2006, p. 60.
8. **Seyedali M**, **Czerniecki JM**, **Morgenroth DC**, **Hahn ME.** Co-contraction patterns of trans-tibial amputee ankle and knee musculature during gait. *J Neuroeng Rehabil* 9: 29, 2012. doi:10.1186/1743-0003-9-29.
9. **Gallina A**, **Peters S**, **Neva JL**, **Boyd LA**, **Garland SJ.** Selectivity of conventional electrodes for recording motor evoked potentials: an investigation with high-density surface electromyography. *Muscle Nerve* 55: 828–834, 2017. doi:10.1002/mus.25412.
10. **Neva JL**, **Gallina A**, **Peters S**, **Garland SJ**, **Boyd LA.** Differentiation of motor evoked potentials elicited from multiple forearm muscles: an investigation with high-density surface electromyography. *Brain Res* 1676: 91–99, 2017. doi:10.1016/j.brainres.2017.09.017.
11. **Rajaratnam BS**, **Ch Goh J**, **Kumar VP.** A comparison of EMG signals from surface and fine-wire electrodes during shoulder abduction. *Int J Phys Med Rehabil* 2: 1–6, 2014. doi:10.4172/2329-9096.1000206.
12. **Van Elswijk G**, **Kleine BU**, **Overeem S**, **Eshuis B**, **Hekkert KD**, **Stegeman DF.** Muscle imaging: mapping responses to transcranial magnetic stimulation with high-density surface electromyography. *Cortex* 44: 609–616, 2008. doi:10.1016/j.cortex.2007.07.003.
13. **Davies JL.** Using transcranial magnetic stimulation to map the cortical representation of lower-limb muscles. *Clin Neurophysiol Pract* 5: 87–99, 2020. doi:10.1016/j.cnp.2020.04.001.
14. **Sazgar M**, **Young MG.** Overview of EEG, electrode placement, and montages. In: *Absolute Epilepsy and EEG Rotation Review*. Cham: Springer International Publishing, 2019, p. 117–125. doi:10.1007/978-3-030-03511-2_5.
15. **Sîmpetru RC**, **Arkudas A**, **Braun DI**, **Osswald M**, **de Oliveira DS**, **Eskofier B**, **Kinfe TM**, **Vecchio AD.** Learning a hand model from dynamic movements using high-density EMG and convolutional neural networks. *IEEE Trans Biomed Eng* 71: 3556–3568, 2024. doi:10.1109/TBME.2024.3432800.
16. **Varghese RJ**, **Pizzi M**, **Kundu A**, **Grison A**, **Burdet E**, **Farina D.** Design, fabrication and evaluation of a stretchable high-density electromyography array. *Sensors (Basel)* 24: 1810, 2024. doi:10.3390/s24061810.
17. **Rojas-Martínez M**, **Mañanas MA**, **Alonso JF**, **Merletti R.** Identification of isometric contractions based on high density EMG maps. *J Electromyogr Kinesiol* 23: 33–42, 2013. doi:10.1016/j.jelekin.2012.06.009.
18. **Rojas-Martínez M**, **Serna LY**, **Jordanic M**, **Marateb HR**, **Merletti R**, **Mañanas MÁ.** High-density surface electromyography signals during isometric contractions of elbow muscles of healthy humans. *Sci Data* 7: 397, 2020. doi:10.1038/s41597-020-00717-6.
19. **Potu BK**, **Kumar V**, **Annam S**, **Sirasanagandla SR.** A morphometric study on flexor carpi radialis muscle of the forearm: a cadaveric study. *Morphologie* 100: 12–16, 2016. doi:10.1016/j.morpho.2015.09.001.
20. **Selvanayagam VS**, **Riek S**, **Carroll TJ.** A systematic method to quantify the presence of cross-talk in stimulus-evoked EMG responses: implications for TMS studies. *J Appl Physiol (1985)* 112: 259–265, 2012. doi:10.1152/japplphysiol.00558.2011.
21. **Parker JL**, **Shariati NH**, **Karantonis DM.** Electrically evoked compound action potential recording in peripheral nerves. *Bioelectron Med* 1: 71–83, 2018. doi:10.2217/bem-2017-0005.
22. **Merletti R**, **Muceli S.** Tutorial. Surface EMG detection in space and time: best practices. *J Electromyogr Kinesiol* 49: 102363, 2019. doi:10.1016/j.jelekin.2019.102363.
23. **Morimoto S**, **Takemori S.** Wave form of motor unit action potential recorded by surface electrode during voluntary muscle contraction. *JPFSM* 3: 191–198, 2014. doi:10.7600/jpfsm.3.191.
24. **Geethanjali P.** Myoelectric control of prosthetic hands: state-of-the-art review. *Med Devices (Auckl)* 9: 247–255, 2016. doi:10.2147/MDER.S91102.
25. **Guzzi G**, **Ricciuti RA**, **Della Torre A**, **Lo Turco E**, **Lavano A**, **Longhini F**, **La Torre D.** Intraoperative neurophysiological monitoring in neurosurgery. *J Clin Med* 13: 2966, 2024. doi:10.3390/jcm13102966.
26. **Mogk JPM**, **Keir PJ.** Crosstalk in surface electromyography of the proximal forearm during gripping tasks. *J Electromyogr Kinesiol* 13: 63–71, 2003. doi:10.1016/s1050-6411(02)00071-8.
27. **Winter DA**, **Fuglevand AJ**, **Archer SE.** Crosstalk in surface electromyography: theoretical and practical estimates. *J Electromyogr Kinesiol* 4: 15–26, 1994. doi:10.1016/1050-6411(94)90023-X.
28. **Mesin L.** Crosstalk in surface electromyogram: literature review and some insights. *Phys Eng Sci Med* 43: 481–492, 2020. doi:10.1007/s13246-020-00868-1.